To be published in Optics Letters:

Title: 106 W, picosecond Yb-doped fiber MOPA system with a radially polarized output beam
Authors: Di Lin,Shaif-Ul Alam,David Richardson,Neda Baktash
Accepted: 14 August 18
Posted 15 August 18
Doc. ID: 340924

106 W, picosecond Yb-doped fiber MOPA system with a radially polarized output beam

DI LIN,* NEDA BAKTASH, SHAIF-UL ALAM, DAVID J. RICHARDSON

[1]*Optoelectronics Research Centre, University of Southampton, SO17 1BJ, UK*
**Corresponding author: Di.Lin@soton.ac.uk*

Received XX Month XXXX; revised XX Month, XXXX; accepted XX Month XXXX; posted XX Month XXXX (Doc. ID XXXXX); published XX Month XXXX

We report the generation of high average output power, high peak power and high pulse energy radially polarized picosecond pulses from a compact gain-switched laser-diode-seeded Yb-doped fiber (YDF) master oscillator power amplifier (MOPA) system. A q-plate was employed as a mode converter prior to the final power amplifier to efficiently convert the linearly polarized Gaussian-shaped beam into a donut-shaped radially polarized beam. The desired vector beam was efficiently amplified yielding ~110ps pulses with a maximum output pulse energy of ~30.7μJ and a peak power of ~280kW at a repetition rate of 1.367MHz. The average power was scaled up to 106W by increasing the repetition rate to 5.468MHz. © 2018 Optical Society of America

OCIS codes: *(060.2320) Fiber optics amplifiers and oscillator; (140.3300) Laser beam shaping; (140.3538) Lasers, pulsed;*

http://dx.doi.org/10.1364/OL.99.099999

Cylindrical vector beams (CVBs) with axially symmetric field-amplitude distributions and radial or azimuthal polarization states have attracted great interest in recent years for a multitude of applications including optical trapping [1], high-resolution imaging [2] and material processing [3, 4]. In the field of material processing high power CVBs have been used to obtain enhanced cutting speeds, to reduce material spatter in deep-penetration welding and to achieve better micro-hole drilling quality [4]. The direct generation of CVBs under both continuous-wave (CW) and pulsed operation at average powers exceeding 100W has been recently demonstrated from a CO_2 laser [5], Nd:YAG rod amplifier [6], thin-disk multipass amplifier [7], and a single crystal fiber amplifier [8]. We recently demonstrated the efficient generation of CVBs from YDF lasers and amplifiers based on conventional few-mode YDFs operating at several tens of watts of average output power in both CW and pulsed modes by employing a nano-grating based spatially variant half-waveplate in the laser cavity/amplifier chain, achieving comparable optical efficiencies to more conventional YDF systems [9-11]. Further power scaling is of interest and the YDF-MOPA architecture, which has previously been demonstrated to provide a compact and robust approach to amplify picosecond pulses to the hundreds of watts of average output power level with diffraction-limited beam [12], represents a promising way to generate high performance, high power CVBs in the picosecond regime.

In this letter, we report a gain-switched laser-diode-seeded YDF-MOPA system capable of generating picosecond pulses with high pulse energy, high peak power and narrow bandwidth in a radially polarized beam at average powers in excess of 100W.

A schematic of the experimental setup is shown in Fig. 1 consisting of a four-stage YDF amplifier chain. The seed is a 1030nm Fabry-Perot laser diode (Oclaro LC96A1030-20R) which is gain-switched using a train of sinusoidal RF pulses at a repetition rate of 87.5MHz. The seed diode is self-seeded using a uniform fiber Bragg grating with a reflectivity of 12.5% to improve the spectral and temporal quality of the gain switched pulses and produces ~150ps, ~4pJ pulses at 1034.7nm with a 3-dB spectral bandwidth of 0.03nm. The first pre-amplifier stage consists of an ~85cm long length of polarization maintaining (PM)-YDF (Nufern PM-YDF-5/130) with a 5μm core diameter and 130μm cladding diameter. It was forward core-pumped by a 975nm single mode laser diode to amplify the pulses to ~20mW average power (signal gain of ~18 dB). A fiber pigtailed electro-optic modulator (EOM) (Photline NIR-MX-LN-10), which has an extinction ratio of ~26dB and an excess insertion loss of ~2.7dB, was used as a pulse picker to reduce the repetition frequency to any desired subharmonic of 87.5 MHz. A second pre-amplifier, having a similar configuration to the first pre-amplifier, was employed after the EOM to ensure adequate seeding of the following cladding-pumped pre-amplifier. A fiber pigtailed acoustic-optic modulator (AOM), synchronized to the EOM, was used to remove inter-pulse amplified spontaneous emission (ASE) which builds up within the prior core-pumped pre-amplifiers. The third pre-amplifier consisted of a ~2.5m long dual-clad PM-YDF (Nufern PLMA-YDF-10/125-VIII) with a core diameter of 10μm (0.085NA) and a cladding diameter of 125μm. This amplifier was forward cladding-pumped with a multimode 975nm pigtailed laser diode.

A free-space band-pass filter (BPF) with a 3-dB bandwidth of 4nm was inserted after the 3rd pre-amplifier to remove any excess out-of-band ASE. The final amplifier comprises a ~2.2 m length commercial few-mode YDF (LIEKKI Yb1200-25/250) which has a core diameter of 25 μm with an NA of 0.075, and an inner cladding diameter of 250 μm with an NA of 0.46. The V-number of the YDF at

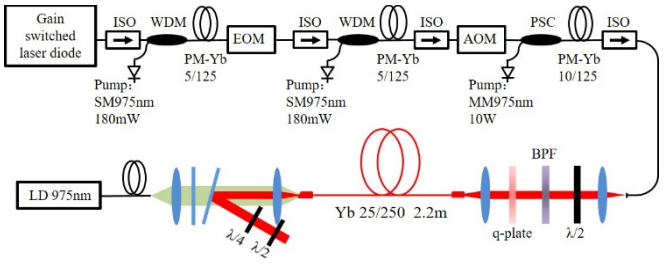

Fig. 1. Schematic of the picosecond YDF-MOPA for amplifying radially polarized beam.

1035nm is 5.3, which means it is capable of supporting the propagation of the two lowest order scalar modes (LP_{01} and LP_{11}). The fiber was loosely coiled with a large bend diameter of ~25cm to avoid any excess propagation loss and to reduce the intermodal coupling as the effective index difference of the four vector modes in the LP_{11} mode group are relatively small. Both ends of the fiber were spliced to ~1.2mm long silica endcaps with a diameter of 250μm to suppress any potential parasitic lasing. The input end facet was perpendicularly-cleaved and the output end facet was angle-cleaved with an angle of ~8 degrees.

A commercially available vortex retarder (also called a q-plate, Thorlabs WPV10L-1064) placed at the input to the final amplifier was employed as the transverse spatial mode converter. The q-plate is composed of a thin liquid crystal polymer film sandwiched between two 1mm thick N-BK7 glass plates with antireflection coatings at 1μm. The q-plate provides a constant half-wavelength retardance at ~1.064μm across its clear aperture, however the orientation (θ) of the fast-axis continuously rotates with respect to the azimuthal angle (φ) over the plate according to the equation: $\theta = \varphi/2 + \delta$ (where δ is the orientation of the fast axis at $\varphi=0$). Therefore, with proper orientation of the q-plate with respect to the incident linearly polarized Gaussian-shaped beam, different CVBs including the radial and azimuthal polarization can be formed. In our case, the q-plate was oriented to convert the input Gaussian beam into a donut-shaped radially polarized beam which was then carefully launched into the final amplifier to excite the radially polarized TM_{01} mode. The q-plate has a high transmission efficiency of >98%, and the resultant converted vector beam experiences negligible degradation in terms of beam quality. A typical converted radially polarized beam measured in the far-field is shown in Fig. 2(a), exhibiting a pronounced donut-shaped intensity profile. The dark-dot in Fig. 2(b) illustrates the measured one dimensional intensity profile across the beam center (red dashed line in Fig. 2(a)), which could be well fitted (red line) with the first higher order Laguerre-Gaussian mode (LG_{01}). The propagation parameter M^2 of the converted donut-shaped beam was measured to be ~2.06, which is very close to the theoretical value of 2 for a radially polarized beam. One of the major advantages of the q-plate is that the resultant donut-shaped mode has negligible intensity at the beam center as shown in Fig. 2 (b). This is critical as any residual intensity at the beam center will be amplified considerably due to the fact that the population inversion in the center of the core is not accessed by the donut-shaped beam, allowing a very high population inversion to be built up at the center of the fiber core. The two-lobed intensity profile beam was passed through a rotated linear polarizer as shown in the Fig. 2(c) indicating that the resultant vector beam should have a high modal purity. The mode extinction ratio (MER) was measured to be ~18dB according to the method described in [10].

In order to get a high peak power pulse with narrow spectral bandwidth, the fiber length and gain of the pre-amplifier chain were optimized such that the self-phase modulation (SPM) induced spectral broadening and stimulated Raman scattering (SRS) induced power transfer to longer wavelength were minimized. Fig. 3 shows the output optical spectra of different pre-amplifier stages measured with an optical spectrum analyzer (OSA) with a low resolution of 2nm. The seed had an optical signal to noise ratio (OSNR) of ~35dB. In order to extract high pulse energy from the MOPA system, the repetition frequency was reduced by a factor of 64 to 1.367MHz with the aid of the EOM. In this case, the EOM introduced a total loss of ~21dB, resulting in a relatively low seeding power of ~100 μW into the second core-pumped pre-amplifier stage. A high gain of ~17dB was extracted from the second pre-amplifier yielding ~5mW of seed signal into the cladding pumped pre-amplifier stage. The EOM in combination with the synchronized AOM effectively suppressed the ASE to ensure that the signal after the core-pumped pre-amplifier stages had a similar OSNR (blue dash line) to that of the seed (black line). An average output power of ~200mW (corresponding to a peak power of 1.3kW) was obtained from the cladding-pumped third pre-amplifier stage. The spectrum (green dash-dot line) shows that it had an OSNR of ~25dB with a component of broadband ASE around 1070nm. In order to avoid seeding SRS in the final power amplifier stage with this broadband ASE, a BPF was employed after the pre-amplifier chain to remove the longer wavelength ASE,

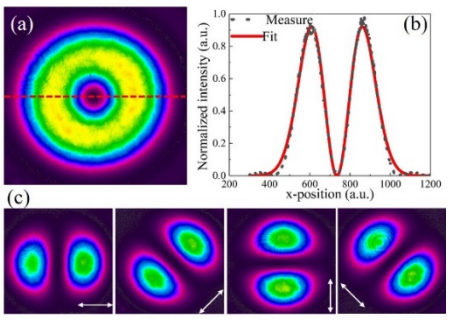

Fig. 2. The donut-shaped radially polarized beam generated by the q-plate.

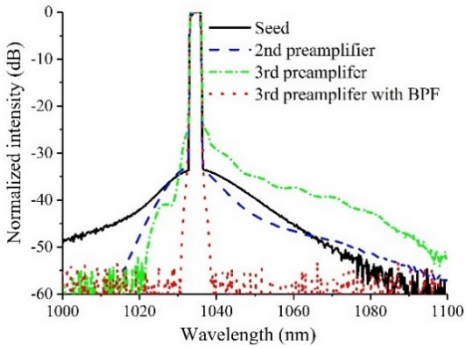

Fig. 3. Spectra (resolution = 2nm) measured after the seed, after the core-pumped preamplifier and cladding-pumped preamplifier stages.

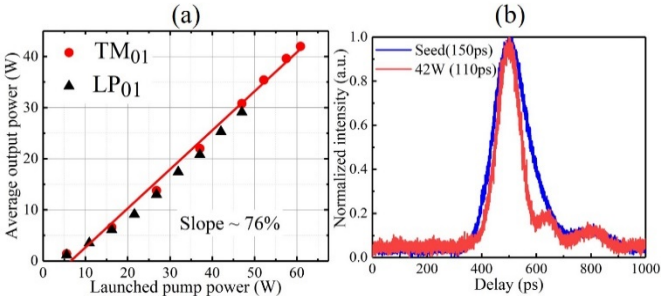

Fig. 4. (a) Average output power of TM_{01} and LP_{01} modes versus the launched pump power. (b) Temporal pulse shapes of the seed (blue) and at maximum TM_{01} output (red).

resulting in a clean narrow band spectra (red dot) that could be used to seed the final amplifier stage.

The q-plate was mounted on an adjustable flip mount so that it could easily be inserted into, or removed from, the signal beam path allowing the MOPA system to be operated either in the donut-shaped TM_{01} mode or in the fundamental LP_{01} mode as required. Fig. 4 (a) shows the average output power of the MOPA system as a function of the launched pump power when operating either on the LP_{01} (black triangle) or TM_{01} (red circle) mode, respectively. A maximum output power of ~42W was obtained for the radially polarized TM_{01} mode at a launched pump power of ~61W, corresponding to a slope efficiency of ~76% with respect to the launched pump power. In comparison, the fundamental LP_{01} mode yielded a maximum output power of ~29W with a similar slope efficiency. The approximately equivalent slope efficiency for the LP_{01} and TM_{01} modes can be attributed to the similar spatial overlap of each mode with the pump beam distribution within the fiber core. Further power scaling was mainly limited by significant nonlinear distortions experienced by the amplified pulses as well as transfer of energy to the SRS line. We stopped further power scaling for both modes when the SRS peak reached a level of ~ -30dB relative to the signal. The temporal profiles of the optical pulses were directly measured by a 32-GHz bandwidth photodetector (Agilent 83440D) and a 20-GHz bandwidth digital communication analyzer (Agilent HP 86100C). The pulse duration of the seed pulses was measured to be ~150ps as shown in Fig. 4(b), and decreased to ~110ps at the maximum output power of 42W, likely due to the strong negative chirp associated with the input seed pulse.

Fig. 5 (a) and (b) show the measured beam intensity profiles in the far-field at the maximum output power for the LP_{01} and TM_{01} modes, respectively. The M^2 values of the LP_{01} and TM_{01} modes were measured to be 1.3 and 2.2, respectively. The donut-shaped intensity profile is well maintained as the output power is increased, and the radial polarization can be preserved with the aid of a pair of half-waveplate and quarter-waveplates at the output as reported in [10, 11]. The bottom row of Fig. 5 shows the intensity distribution of the TM_{01} mode when passed through a rotated linear polarizer. The MER was measured to be ~10dB at 42W.

A comparison of the output optical spectrum (0.5 nm resolution) for both the LP_{01} and TM_{01} modes at the maximum output power is illustrated in Fig. 6(a). It clearly indicates that the donut-shaped TM_{01} mode has a higher SRS threshold than the fundamental LP_{01} mode. For the LP_{01} mode (black line), the SRS peak at ~1090nm becomes apparent (~30dB below the signal peak) when the average output power reaches ~29W corresponding to a pulse energy of 21.2μJ and a peak power of ~190kW. However, at the same SRS peak suppression, the average output power of the TM_{01} mode (red line) can be scaled up to 42W corresponding to a pulse energy of 30.7μJ and a peak power of ~280kW. Our results show that ~45% of additional pulse energy can be extracted for the donut-shaped TM_{01} mode than the fundamental LP_{01} mode. This is mainly due to the significantly larger effective mode area of the TM_{01} mode. Our calculations show that for the few-mode YDF used in our setup, the TM_{01} mode has an effective mode area of ~460μm^2, which is 40% larger than the LP_{01} mode (~330 μm^2), consistent with our SRS observations. Fig. 6(b) plots the spectral profiles of each transverse mode with an OSA resolution of 0.02nm at the maximum output power. The 3-dB bandwidth of the output pulse was broadened to 0.69nm for the LP_{01} mode (black line) and 0.73nm for the TM_{01} mode (red line) due mainly to SPM (maximum acquired nonlinear phase shift of 6.5π). It is clear however that the detailed nonlinear spectral evolution of the TM_{01} mode and the LP_{01} mode are somewhat different, likely due to the presence of four-wave mixing (FWM) for the LP_{01} mode operation. This could be attributed to the presence of the LP_{11} mode as the M^2 value of LP_{01} mode was 1.3. The two modes have different dispersive properties likely resulting in enhanced phase-matching contributions to the

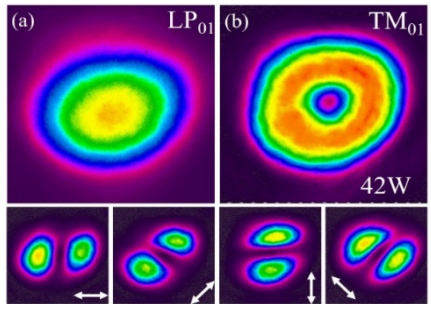

Fig. 5. Typical beam profiles at maximum output power (a) LP_{01} mode at 29W, (b) TM_{01} mode at 42W. The bottom row shows the beam intensity distributions of TM_{01} mode passing through a rotated linear polarizer.

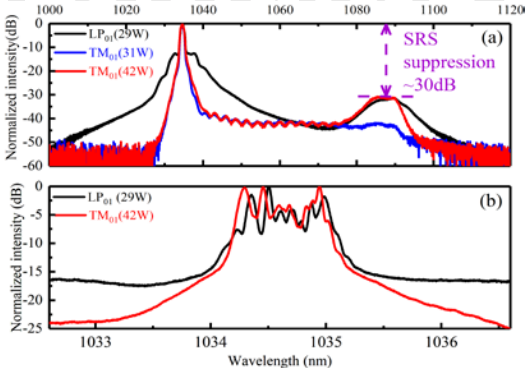

Fig. 6. (a) Spectra (resolution = 0.5nm) measured for LP_{01} and TM_{01} modes at different output powers. (b) Spectra (resolution = 0.02nm) measured at the maximum output power of LP_{01} mode (black line) and TM_{01} mode (red line).

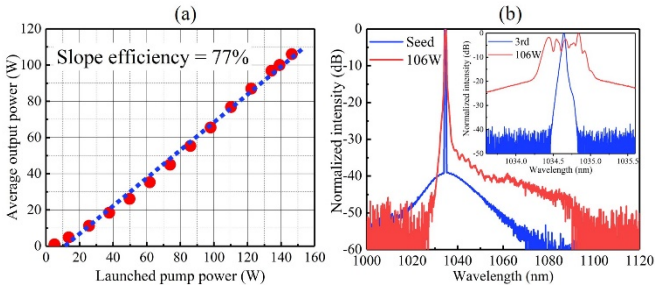

Fig. 7. (a) Average output power of TM_{01} mode at a repetition rate of 5.45MHz versus the launched pump power; (b) spectra (resolution= 0.5nm) measured for the seed and maximum output power of 106W. The insert shows the corresponding spectra measured with a resolution of 0.02nm.

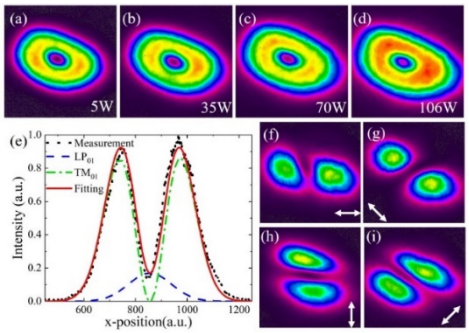

Fig. 8. (a)-(d) The measured intensity profiles of the radially polarized beam at different output powers; (e) one dimensional intensity profile across the beam center at 106W fitted with an incoherent superposition of LP_{01} and TM_{01} modes;(f)-(g) the beam intensity distributions after passing through a rotated linear polarizer.

FWM process [13]. By integrating the spectra in Fig. 6(b), we estimated that ~56% of the total pulse energy was contained within the 3-dB bandwidth for the LP_{01} mode. In comparison, ~80% of the total pulse energy was contained within the 3-dB bandwidth for the TM_{01} mode.

To further scale the average output power of the radially polarized TM_{01} mode, the repetition rate of the MOPA system was increased by four times to 5.468MHz. In this case, an average power of ~500mW of donut-shaped radially polarized beam was obtained after the pre-amplifier chain which was then coupled into the final power amplifier stage. As shown in Fig. 7(a), the average output power of the donut-shaped TM_{01} mode was linearly increased to ~106W corresponding to a gain of ~23.3dB and slope efficiency of 77% with respect to the launched pump power. This corresponds to a maximum pulse energy of ~19.4μJ with a peak power of ~176kW. Fig. 7 (b) shows the measured spectral profiles of the seed and output beam at the maximum output power of 106W with an OSA resolution of 0.5nm and 0.02nm (insert), respectively. The spectra indicates that both the ASE and SRS were well suppressed. The 3dB bandwidth was broadened to 0.46nm containing ~80% of total pulse energy. The evolution of the beam intensity distribution of the TM_{01} mode as a function of output power is shown in the Fig. 8(a)-(d). The beam profile exhibits a pronounced donut-shape with slight ellipticity and little variation at different power levels. The ellipticity is believed to be due to the aberration induced to the output beam resulting from slight deviation of the output beam from the optic axis due to the slightly curved angle-cleaved fiber end facet. The intensity at the beam center gradually increases with an increase in output power, and becomes quite appreciable at the maximum output power of 106W as shown in Fig. 8(d). Fig. 8(e) plots the one-dimensional intensity profile across the beam center for Fig. 8(d). The measured intensity profile (black dots) was fitted using an incoherent superposition of LP_{01} and TM_{01} modes (red line), indicating that ~7% of power appears to be in the LP_{01} mode. This could be attributed to the fast build-up of ASE as well as amplification of the residual LP_{01} mode under high pump power conditions. The MER was deteriorated to ~8dB, and the M^2 was measured to be 2.38 at the maximum output power.

In summary, we demonstrated a gain-switched diode-seeded YDF-MOPA system capable of generating high average output power, high pulse energy and high peak power picosecond pulses with a radially polarized donut beam profile. The maximum pulse energy reached to 30.7μJ with a peak power of ~280kW at a repetition rate of 1.367MHz. The extracted pulse energy in the radially polarized mode is ~45% higher than the fundamental LP_{01} mode. The average output power of the radially polarized beam was further scaled up to 106W at a repetition rate of 5.467MHz, corresponding to a pulse energy of ~19.4μJ and a peak power of ~176kW. To the best of our knowledge, this is the highest average output power and highest peak power obtained for CVB from a conventional step-index few-mode fiber laser. Such a high average power, high peak power and high pulse energy CVB source should be attractive for a variety of applications in high-throughput material processing and imaging.

The data from this Letter is available at repository: https://doi.org/10.5258/SOTON/D0622

Funding. Engineering and Physical Sciences Research Council (EPSRC) (EP/P012248/1).

REFERENCES

1. T. Kuga, Y. Torii, N. Shiokawa, T. Hirano, Y. Shimizu, and H. Sasada, Phys. Rev. Lett. **78**, 4713 (1997).
2. L. Novotny, M. R. Beversluis, K. S. Youngworth, and T. G. Brown, Phys. Rev. Lett. **86**, 5251 (2001).
3. M. Kraus, M. A. Ahmed, A. Michalowski, A. Voss, R. Weber, and T. Graf, Opt. Express **18**, 22305 (2010).
4. R. Weber, A. Michalowski, M. Abdou-Ahmed, V. Onuseit, V. Rominger, M. Kraus, and T. Graf, Phys. Procedia **12**, 21 (2011).
5. M. A. Ahmed, Opt. Lett. 32, 1824-1826 (2007).
6. I. Moshe, S. Jackel, A. Meir, Y. Lumer, and E. Leibush, Opt. Lett. **32** (2007).
7. A. Loescher, J. P. Negel, T. Graf, and M. A. Ahmed, Opt. Lett. **40**, 5758 (2015).
8. S. Piehler, X. Delen, M. Rumpel, J. Didierjean, N. Aubry, T. Graf, F. Balembois, P. Georges, and M. A. Ahmed, Opt. Express **21**, 11376 (2013).
9. D. Lin, J. M. O. Daniel, and W. A. Clarkson, Opt. Lett. **39**, 3903 (2014).
10. D. Lin, N. Baktash, M. Berendt, M. Beresna, P. G. Kazansky, W. A. Clarkson, S. U. Alam, and D. J. Richardson, Opt. Lett. **42**, 1740 (2017).
11. B. M. Zhang, Y. J. Feng, D. Lin, J. H. V. Price, J. Nilsson, S. Alam, P. P. Shum, D. N. Payne, and D. J. Richardson, Opt. Express **25**, 15402 (2017).
12. P. S. Teh, S. U. Alam, R. J. Lewis, and D. J. Richardson, Laser Phys. Lett. **11**, 085103 (2014).
13. G. P. Agrawal, *Nonlinear Fiber Optics*, (Academic Press, 2013)

Reference

1. T. Kuga, Y. Torii, N. Shiokawa, T. Hirano, Y. Shimizu, and H. Sasada, "Novel optical trap of atoms with a doughnut beam," Physical Review Letters **78**, 4713-4716 (1997).
2. L. Novotny, M. R. Beversluis, K. S. Youngworth, and T. G. Brown, "Longitudinal field modes probed by single molecules," Physical Review Letters **86**, 5251-5254 (2001).
3. M. Kraus, M. A. Ahmed, A. Michalowski, A. Voss, R. Weber, and T. Graf, "Microdrilling in steel using ultrashort pulsed laser beams with radial and azimuthal polarization," Optics Express **18**, 22305-22313 (2010).
4. R. Weber, A. Michalowski, M. Abdou-Ahmed, V. Onuseit, V. Rominger, M. Kraus, and T. Graf, "Effects of Radial and Tangential Polarization in Laser Material Processing," Physcs Proc **12**, 21-30 (2011).
5. M. A. Ahmed, "Radially polarized 3 kW beam from a CO2 laser with an intracavity resonant grating mirror," Optics Letters **32**, 1824-1826 (2007).
6. I. M. E. Leibush, "2kW M2 less than 10 radially polarized beams from aberration-compensated rod-based Nd：YAG lasers," Optics Letters **32** (2007).
7. A. Loescher, J. P. Negel, T. Graf, and M. A. Ahmed, "Radially polarized emission with 635 W of average power and 2.1 mJ of pulse energy generated by an ultrafast thin-disk multipass amplifier," Optics Letters **40**, 5758-5761 (2015).
8. S. Piehler, X. Delen, M. Rumpel, J. Didierjean, N. Aubry, T. Graf, F. Balembois, P. Georges, and M. A. Ahmed, "Amplification of cylindrically polarized laser beams in single crystal fiber amplifiers," Optics Express **21**, 11376-11381 (2013).
9. D. Lin, J. M. O. Daniel, and W. A. Clarkson, "Controlling the handedness of directly excited Laguerre-Gaussian modes in a solid-state laser," Optics Letters **39**, 3903-3906 (2014).
10. D. Lin, N. Baktash, M. Berendt, M. Beresna, P. G. Kazansky, W. A. Clarkson, S. U. Alam, and D. J. Richardson, "Radially and azimuthally polarized nanosecond Yb-doped fiber MOPA system incorporating temporal shaping," Optics Letters **42**, 1740-1743 (2017).
11. B. M. Zhang, Y. J. Feng, D. Lin, J. H. V. Price, J. Nilsson, S. Alam, P. P. Shum, D. N. Payne, and D. J. Richardson, "Demonstration of arbitrary temporal shaping of picosecond pulses in a radially polarized Yb-fiber MOPA with > 10 W average power," Optics Express **25**, 15402-15413 (2017).
12. P. S. Teh, S. U. Alam, R. J. Lewis, and D. J. Richardson, "Single polarization picosecond fiber MOPA power scaled to beyond 500 W," Laser Physics Letters **11** (2014).
13. G. P. Agrawal, "Nonlinear Fiber Optics," (2013).